South Asian summer monsoon enhanced by the uplift of Iranian Plateau in Middle Miocene

Meng Zuo[1,2], Yong Sun[3], Yan Zhao[3*], Gilles Ramstein[4], Lin Ding[3], Tianjun Zhou[1]

1 LASG, Institute of Atmospheric Physics, Chinese Academy of Sciences, Beijing, China

2 State Key Laboratory of Severe Weather and Institute of Tibetan Plateau Meteorology, Chinese Academy of Meteorological Sciences, Beijing, China

3 Key Laboratory of Continental Collision and Plateau Uplift, Institute of Tibetan Plateau Research, and Center for Excellence in Tibetan Plateau Earth Sciences, Chinese Academy of Sciences, Beijing 100101, China

4 Laboratoire des Sciences du Climat et de l'environnement, CNRS-CEA-UVSQ, 91191 Gif-sur-Yvette, France

Correspondence: Yan Zhao (yan.zhao@itpcas.ac.cn)

ABSTRACT

The South Asian summer monsoon (SASM) significantly intensified during the Middle Miocene (17-12 Ma), but the driver of this change remains an open question. The uplift of the Himalaya (HM) and the Iranian Plateau (IP), and global CO_2 variation are prominent factors among suggested drivers. Particularly, the impact of high CO_2 levels on the Miocene SASM has been little studied, despite the wide range of reconstructed CO_2 values around this period. Here we investigate their effects on the SASM using the fully coupled Ocean-Atmosphere Global Climate Model CESM1.2 through a series of 12 sensitivity experiments. Our simulations show that the IP uplift plays a dominant role in the intensification of the SASM, mainly in the region around northwestern India. The effect of the HM uplift is confined to the range of the HM and its vicinity, producing orographic precipitation change. The topography forcing overall out-competes CO_2 variation in driving the intensification of the SASM. In the case of extremely strong CO_2 variation, the effects of these two factors are comparable in the core SASM region, while in the western region, the topographic forcing is still the dominant driver. We propose a thermodynamical process linking the uplift of the IP and the enhanced SASM through the release of latent heat. Compared with reconstructions, the simulated response of SASM to the IP uplift is in good agreement with observed precipitation and wind filed, while the effects of the HM uplift and CO_2 variation are inadequate to interpret the proxies.

Keywords: South Asian summer monsoon, Middle Miocene, topographic change, CO_2 variation, thermal heating effect

1. Introduction

The Middle Miocene (17-12 Ma) was a period characterized by major climatic, tectonic, CO_2 and environmental changes (Steinthorsdottir et al., 2021). Increasing evidence indicates that the South Asian summer monsoon (SASM) was remarkably intensified in the Middle Miocene (Clift et al., 2008; Clift and Webb, 2019; Gupta et al., 2015; Bialik et al., 2020; Bhatia et al., 2021; Vogeli et al., 2017) although its inception was no later than the Early Miocene (Ali et al. 2021, Licht, 2014; Farnsworth et al., 2019). However, the driving factor of its evolution remains an issue of great debate. Besides the effect of geographic change (Ramstein et al., 1997; Fluteau et al., 1999; Farnsworth et al., 2019; Thomason et al., 2021; Tardif et al., 2020, 2023; Sarr et al., 2022), the growth of the Himalaya (HM)-Tibetan Plateau (TP; HM-TP) has traditionally been called for the SASM development (Cliff et al., 2008; Clift and Webb, 2019; Manabe and Terpstra, 1974; Kutzbach et al., 1989; Prell and Kutzbach, 1992; Ramstein et al., 1997; An et al., 2001; Kitoh, 2002; Chakraborty et al., 2006; Wu et al., 2012; Tada et al., 2016; Tarif et al., 2020, 2023). The HM, which has long been regarded as the "southern TP" (Spicer, 2017), receives particular attention (Boos and Kuang, 2010; Wu et al., 2012; Zhang et al., 2015). Recent geological evidence (Liu et al., 2016; Ding et al., 2017, 2022) suggests that, in contrast to previous studies, the HM had risen to a height of 2.3 ± 0.9 km by the earliest Miocene, reaching approximately 4 km by 19 Ma. From 15 Ma onwards, the HM projected significantly above the average elevation of the plateau that had already attained its modern height before the Miocene (Wang et al., 2014). The coincidence of the ongoing HM uplift above the TP since 15 Ma and the intensification of SASM appears to support the hypothesis that the evolution of the SASM is predominantly driven by the formation of HM-TP.

However, this traditional view is challenged by many modeling studies that emphasize the importance of peripheral mountain ranges (Chakraborty et al., 2006; Tardif et al., 2020, 2023; Sarr et al., 2022; Liu et al., 2017; Tang et al., 2013; Chen et al., 2014; Acosta and Huber, 2020). Notably, the Iranian Plateau (IP), which also underwent uplift during the same period as the Miocene SASM enhancement around 15-12 Ma, is considered a critical factor (McQuarrie et al., 2003; Mouthereau, 2011; Ballato et al., 2017；Bialik et al., 2020), although the evolution history of the IP's build-up remains hotly debated (Agard et al., 2011; McQuarrie et al., 2003; Mouthereau, 2011; Ballato et al., 2017). Nevertheless, most studies suggest a Miocene age for the uplift of most landforms. Geological evidence indicates that in the northern sectors of the IP, the uplift likely occurred between 16.5-10.7 Ma (Ballato et al., 2017), particularly accelerated after 12.4 Ma (Mouthereau, 2011) while in regions bordering the IP to the south, uplift occurred between 15 and 5 Ma (Mouthereau, 2011). The Zagros orogen, a significant part of the IP, developed in three distinct pulses within the last ~20 Ma (Agard et al., 2011; Mouthereau, 2011). Therefore, there exists significant uncertainty regarding the growth of the IP. The respective contributions of the IP and HM uplift to intensified SASM during the Middle Miocene remain unclear.

Various mechanisms were proposed to explain the linkage between the uplift of the IP and HM and the intensification of SASM rainfall. These include the mechanical blocking effect (Tang et al., 2013), topographic thermal forcing (Chen et al., 2014; Wu et al., 2012; Liu et al., 2017), and the role of gatekeeper to insulate the pool of high-enthalpy air in northern India from westerly advection of cool and dry air (Acosta and Huber, 2020). However, most of these modeling studies have examined the effects of IP and HM uplift using Atmospheric General Circulation Model (AGCM) with modern geographies (Liu et al., 2017; Zhang et al., 2015; Tang et al., 2013; Acosta and Huber, 2020), potentially overlooking two key factors: 1) the neglect of air-sea interaction processes (Kitoh, 2002; Su et al., 2018); 2) the risk of misinterpreting past changes due to the critical role of land-sea distribution in shaping the paleoclimate features (Tardif et al., 2023; Ramstein et al., 1997). Therefore, we opt to use a fully coupled Ocean-Atmosphere Global Climate Model (OAGCM) to revisit the response of the SASM to the IP and HM uplift under Miocene boundary conditions despite requiring additional computational resources.

The SASM is sensitive to changes in CO_2 concentration (Thomson et al., 2021). The effect of CO_2 variation is overall estimated to be less than that of geography and/or topography (Farnsworth et al., 2019; Thomson et al., 2021; Tardif et al., 2023), however, during the mid-to-late Miocene, its contribution to rainfall change is comparable to that of orographic uplift even when the CO_2 is set from 560 ppm to 280 ppm (Thomson et al., 2021). Proxy records indicate that the early to middle Miocene was a warming period, which is known as the Middle Miocene Climatic Optimum (∼17-14 Ma), followed by a late Miocene cooling (Steinthorsdottir et al., 2021). There is large uncertainty in estimated CO_2 variation in the Middle Miocene, with a wide range of reconstructed values from ∼180 ppmv to ∼600 ppmv (Foster and Rohling, 2013; Pagani et al., 1999; Steinthorsdottir et al., 2021; The CenCO_2PIP, 2023, and reference herein), even to more than 1000 ppmv (Rae et al., 2021) during the Middle Miocene Climatic Optimum. Nevertheless, according to general concept, the atmospheric CO_2 concentration peaked around 15 Ma and then declined (The CenCO_2PIP, 2023). Therefore, it is necessary to re-examine the effect of CO_2 forcing on SASM rainfall based on the possible range of CO_2 variation.

In this study, we utilize a fully coupled OAGCM to explore the impact of IP and HM uplift and the CO_2 variation on the SASM. Considering that the uplift of HM and IP predominantly occurred after 15 Ma, roughly coinciding with pronounced CO_2 variations during 17-14 Ma, we conduct two sets of sensitivity experiments based on Middle Miocene geography. The topographic sensitivity experiments are placed into the context of the current understanding of the regional tectonic and geographic settings while a set of CO_2 sensitivity experiments ranging from 280 to 1000 ppmv is performed. The model configuration, Middle Miocene boundary condition and experimental design are described in Section 2. In Section 3, we show the SASM response to IP and HM uplift, and the effect of CO_2 forcing. The mechanisms responsible for the monsoonal precipitation change are examined in Section 4. The implication of our results to the evolution of the SASM in the Middle Miocene is discussed in Section 5 before giving conclusions in Section 6.

2. Data and Methods

2.1. Climate model

The model used in this study is the Community Earth System Model (CESM), Version 1.2.1 of the National Center for Atmospheric Research. It includes the Community Atmosphere Model (CAM4) (Neale et al., 2013), the Community Land Model (CLM4; Hunke and Lipscomb, 2010), the Parallel Ocean Program (POP2; Smith et al., 2010), the Community Ice Sheet Model and the Community Ice code (Glimmer-CICE4). Both the Ice sheet Model and the dynamic vegetation module (Lawrence et al., 2011) incorporated in CLM4 are switched off in this study. The horizontal resolution used is 1.9°(latitude) × 2.5° (longitude) for CAM4 with 26 vertical levels and CLM4 has identical horizontal resolution. CESM has been extensively used for modern and the tectonic climate studies (Chen et al., 2014; Goldner et al., 2014; Frigola et al., 2018）. In general, this model simulates modern surface temperature distributions and equator-to-pole temperature gradients well (Gent et al., 2011), although biases exist (Neale et al., 2013). However, it strongly overestimates the Miocene meridional temperature gradient compared to reconstructions, a thorny problem for Miocene modeling practice (Burls et al., 2021; Steinthorsdottir et al., 2021) mainly caused by the inability of climate models to reproduce polar amplified warmth (Krapp and Jungclaus, 2011; Herold et al., 2011; Goldner et al., 2014; Burls et al., 2021). Nevertheless, the temperature biases in low latitudes are small, generally within 1°C (Burls et al., 2021).

2.2. Boundary conditions

Our Miocene experiments are configured with geography, topography, bathymetry and vegetation cover from Frigola et al. (2018, henceforth F18), which provides boundary conditions for modeling studies with a focus on the Middle Miocene. According to F18, the most prominent geographic differences between the Middle Miocene and present day are the opening of the Tethys, Indonesian and Panama seaways, the closure of the Bering Strait and lower elevations of most of the highest regions of the globe. For instance, the African topographies were reduced to 25% of its current elevation (Figs. 1a and b).

The topography of the Tibetan Plateau in F18 is set to its estimated Early to Middle Miocene elevation. The southern and central plateau reached a near modern elevation, the northern plateau is set to 3-4 km but its northward extend is reduced to reflect the rapid uplift occurring in Pliocene (Harris, 2006, and the references therein). The HM reached to 60-80% of its present height. As for the IP, here we lumped together all the mountain ranges west of the Himalayan, including the Hindu Kush region and Pamir as the IP. In F18, the northern part of the IP reached a near modern elevation as 1000-2000 m, but its southern part was lower than 1000 m.

The Miocene vegetation is prescribed as that in F18, which is a global gridded distribution (Figure S1 in Supplementary Materials (SM)) merging previous reconstructions (See F18 for more details). During the Miocene, vegetation types associated with lower latitudes today encroached on higher latitudes. There was reduced presence of ice compared to modern conditions, and ice-free regions were covered by tundra in Antarctica while cold mixed forests spread over Greenland.

2.3. Experimental design

We first perform two simulations: the pre-industrial (piControl) and the Middle Miocene (MMIO) simulation, which differ in their applied geography (Figs. 1a and b), bathymetry, vegetation cover and the CO_2 concentrations while the solar constant, orbital configuration and the concentrations of other greenhouse gases are kept at their modern values. The CO_2 concentration is set to 280 ppmv in the piControl (Eyring et al., 2016) and 400 ppmv in the MMIO following the setting of F18. The choice of 400 ppmv is somewhat low but within the range of published estimates (see details in F18 and Burls et al., 2021). Both simulations are integrated to reach quasi-equilibrium, particularly the MMIO experiment is integrated ca 3000 years. The difference between MMIO and piControl provides the background information of the simulated changes in the SASM between the two periods.

Starting from the MMIO simulation, we run a set of experiments with altered orography in the HM and the IP. We examine the joint effects of the HM and IP on the SASM assuming the HM and the IP rise simultaneously from flat (0%) to 100% of their reference height (Figs. 1c and d). The reference height is the modern altitude for the HM and the reconstructed Miocene altitude for the IP. The experiments are referred as IP0HM0 and IP100HM100, respectively. To further separate the climatic effect of the IP and HM uplift, we conduct another two experiments: IP100HM0 and IP0HM100. In the former (latter) experiment, the HM (IP) is absent while the IP (HM) reaches its reference height (Figs.1e and f). Combined with the experiments of IP0HM0 and IP100HM100, the effect of elevated IP and HM is estimated (see section 3.2). To further reveal the impact of the IP uplift on the SASM evolution, two other experiments are conducted: IP50HM0 and IP50HM100, indicating that the IP is reduced by half of its Miocene height while the HM is absent and fully uplifted, respectively.

To clarify the relative role of CO_2 forcing on SASM rainfall in the Middle Miocene, we also run a set of CO_2 sensitivity experiments with the CO_2 setting to 280, 560, 800 and 1000 ppmv, referred to as MMIO280, MMIO560, MMIO800 and MMIO1000, respectively. The high values as 800 and 1000 ppm are chosen because new reconstructions of CO_2 are generally corresponded to 3 times the pre-industrial levels (Rae et al., 2021). These experiments share the same boundary conditions as the MMIO simulation, differing only in CO_2 concentration.

The simulations considered in our study are listed in Table 1. The sensitivity experiments are integrated from the MMIO equilibrium state for another 200 (500) years for the topography (CO_2) sensitivity experiments to reach quasi-equilibrium. The final 50 years of these simulations are used for analysis.

2.4. South Asian Summer Monsoon indices

The following indices are defined to illustrate features of the SASM changes.

(1) All Indian rainfall (AIR): regional summer mean precipitation over the land points within the domain of 7-30°N, 65-95°E. It represents the precipitation in the core region of the SASM.

(2) Webster-Yang Index (WYI; Webster and Yang, 1992): meridional wind stress shear between 850 hPa and 200 hPa averaged over 40-110°E, 0-20°N during June-August.

(3) Somali jet strength (SMJ; Sarr at al., 2022): Maximum intensity of the Somali jet over the Arabian Sea (averaged over 30-60°E, 0-20°N) during June-August.

2.5. Moisture budget analysis

Moisture budget analysis (MDA) can decompose the precipitation change into changes in evaporation and moisture advection (Chou et al. 2009). It relates the net precipitation (precipitation minus evaporation; P - E) to the vertically integrated moisture flux convergence (Chou et al., 2009). More details about MDA are given in SM 2. This method has been widely applied to paleoclimate studies in recent years, such as distinguishing the physical processes involved in precipitation changes in Mid-Holocene (Sun et al., 2023). Here, we apply MDA to reveal the physical processes related to SASM precipitation responses to the uplift of IP-HM and to CO_2 change.

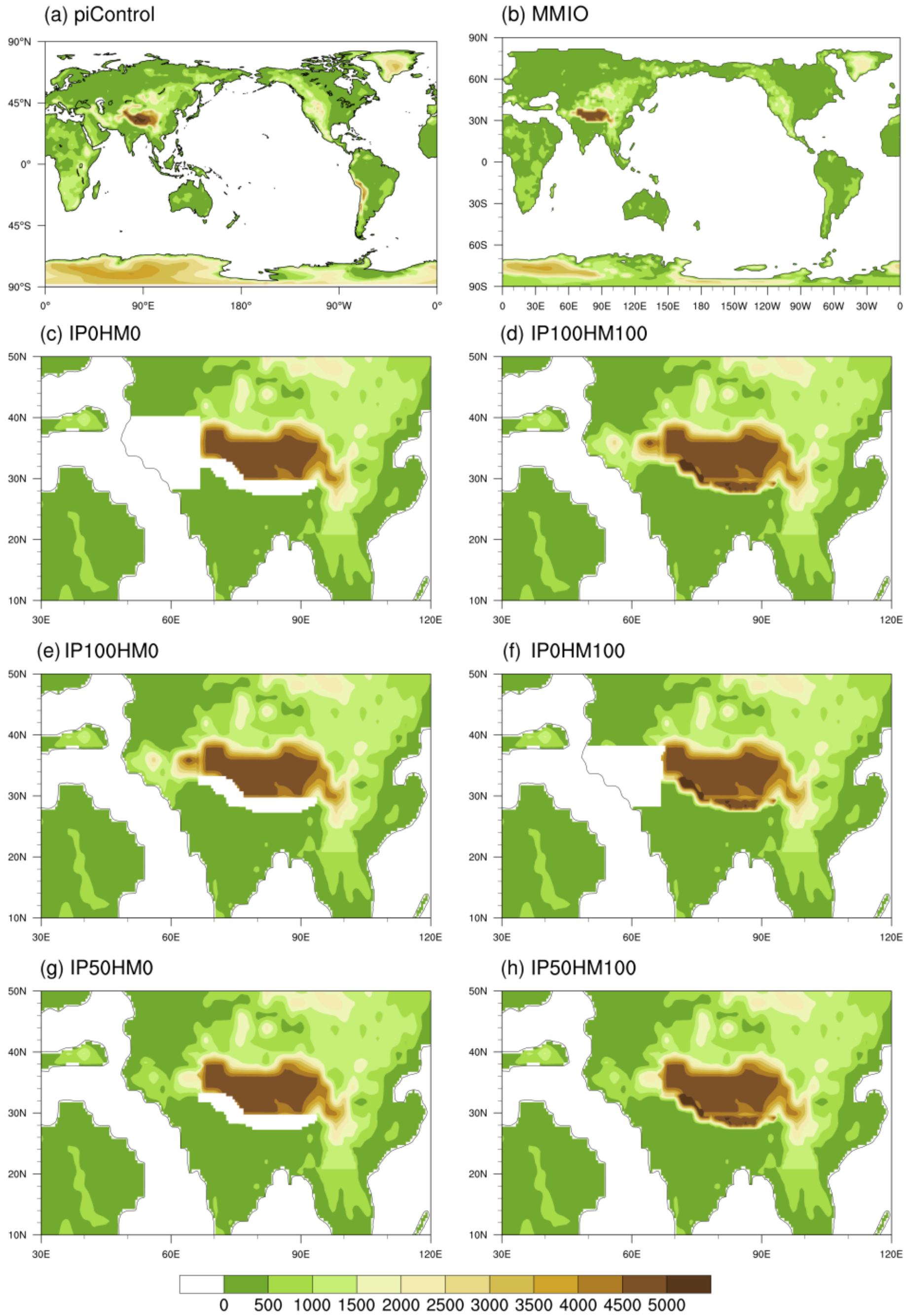

Figure 1. Topography of (a) piControl, (b) MMIO and orographic sensitivity experiments, including (c) IP0HM0, (d) IP100HM100, (e) IP100HM0 and (f) IP0HM100, (g) IP50HM0, (h) IP50HM100 (The maps are plotted at 0.5°×0.5° resolution. The same maps but at 1.9°×2.5° resolution are provided in the SM as Fig. S2)

3. Results

3.1. Climatology of the SASM in the present day and Middle Miocene

The CESM1.2 is one of the best models in simulating the present-day SASM (Anand et al., 2018; Jin et al., 2020). The CESM1.2 reproduced the broad features of the SASM system including the onshore flows and strong monsoonal precipitation when compared to the observational datasets including GPCP (precipitation) and ERA5 (circulation) (Huffman et al., 2009; Hersbach et al. 2020). The maximum centers of precipitation are reasonably captured over the southern slope of the HM, the East Arabian Sea and Bay of Bengal despite biases in intensity and extensions (Figs. 2a, b), which is largely due to the coarse spatial resolution (Acosta and Huber, 2017**;** Anand et al., 2018; Botsyun et al., 2022a, b; Boos and Hurley, 2012). Thus, we focus on the large-scale circulations and treat the local features with caution. The regional summer mean precipitation, as measured by the AIR, is 7.7 mm day^{-1} in GPCP and 8.7 mm day^{-1} in the piControl experiment. The positive bias reflects an overestimation of precipitation in the Western Ghats and at the HM foothills.

Compared with the piControl experiment, the MMIO simulation displays apparent adjustment of the JJA mean low-level circulation. The westerlies pass Africa into the Indian region, and a cyclonic circulation develops over the Arabian Sea, the cross-equatorial flow weakens and displaces southward (Fig. 2c). There is considerable enhancement of monsoonal precipitation in South Asia but not limited there (Fig. 2c). AIR in MMIO simulation is 10.4 mm day^{-1}, which is ~20% higher than that in piControl experiment.

The wetter Miocene climate is also reflected by the widespread Africa-Asian monsoon, which was suggested by previous modeling studies (Herold and Huber, 2011; Zhang et al., 2015). Here a monsoon-like climate is defined as local summer-minus-winter precipitation exceeding 2 mm day^{-1} and the local summer precipitation exceeding 55% of the annual total (Wang and Ding, 2008). This monsoon index is determined by the intensity of summer monsoonal precipitation in the region of the South Asian Monsoon (SAM). Compared with present day, the domain of the SAM extends westward both in land and over the Arabian Sea where it nearly connects the African monsoon (Fig. 3c). Interestingly, this characteristic is also noted in the Miocene study of Fluteau et al. (1999), despite significant differences in the climate model and paleogeography employed in the two studies. The distribution of the simulated SAM is generally consistent with the proxies (Table 2), confirming the wide existence of SAM in the Middle Miocene in terms of rainfall seasonality.

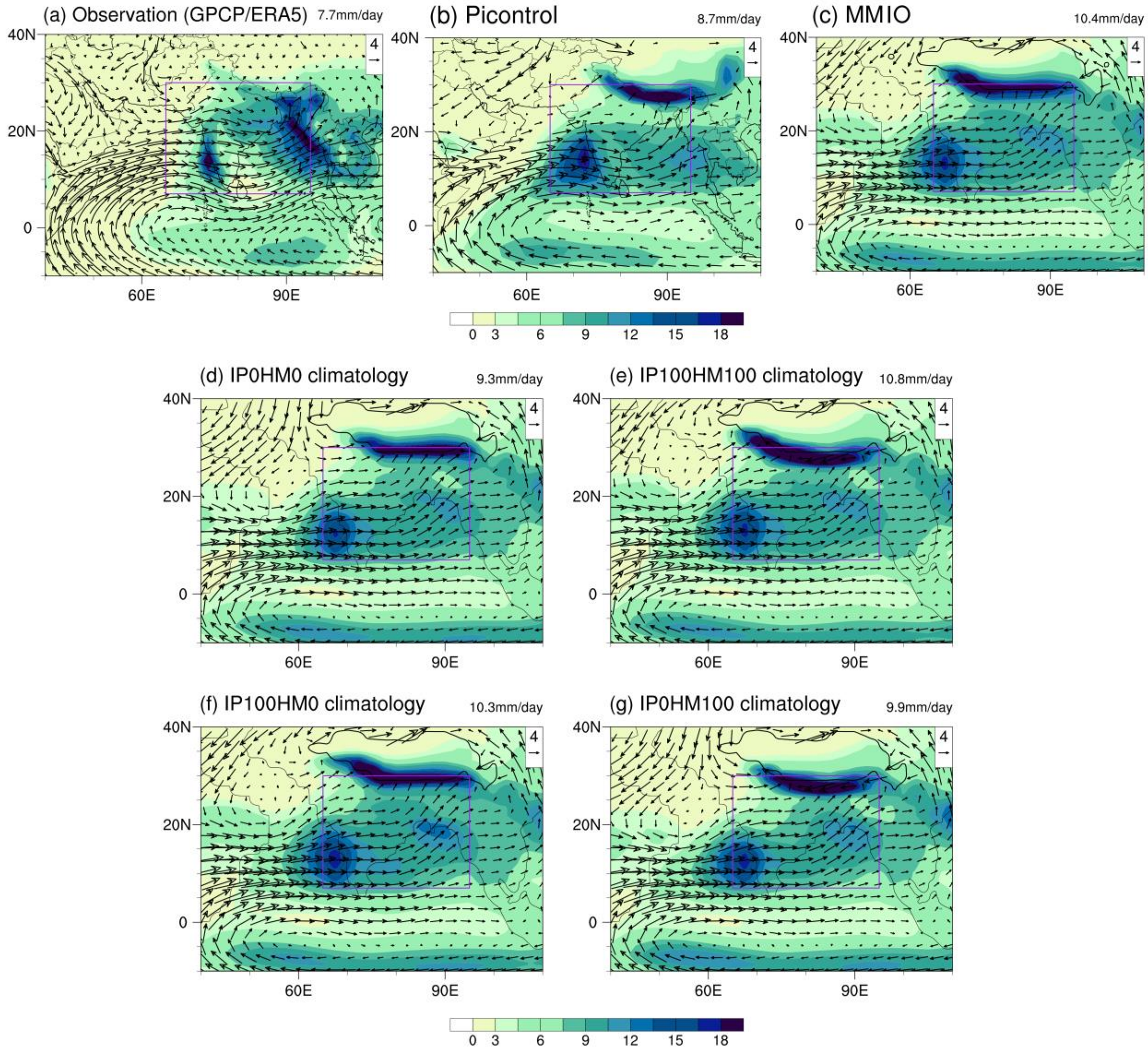

Figure 2. Climatology of JJA (June-July-August) seasonal mean South Asia summer monsoon (SASM) precipitation (mm day^{-1}) and 850 hPa winds (vectors, m s^{-1}) from (a) observation precipitation from GPCP and circulation from ERA5), (b) Preindustrial control experiment and (c) MMIO experiment. (d) IP0HM0, (e) IP100HM100, (f) IP100HM0, (g) IP0HM100. Climatology is the average over 1979-2005 for the observation. As for the piControl and MMIO experiment, we select the last 50 and 100 years of simulation, respectively. All Indian rainfall (AIR) is shown at the top-right of each panel. AIR indicates precipitation over the land points within the purple square in each panel (7-30°N, 65-95°E). The black contour in panel (c)-(g) indicates the altitude of 2500 m.

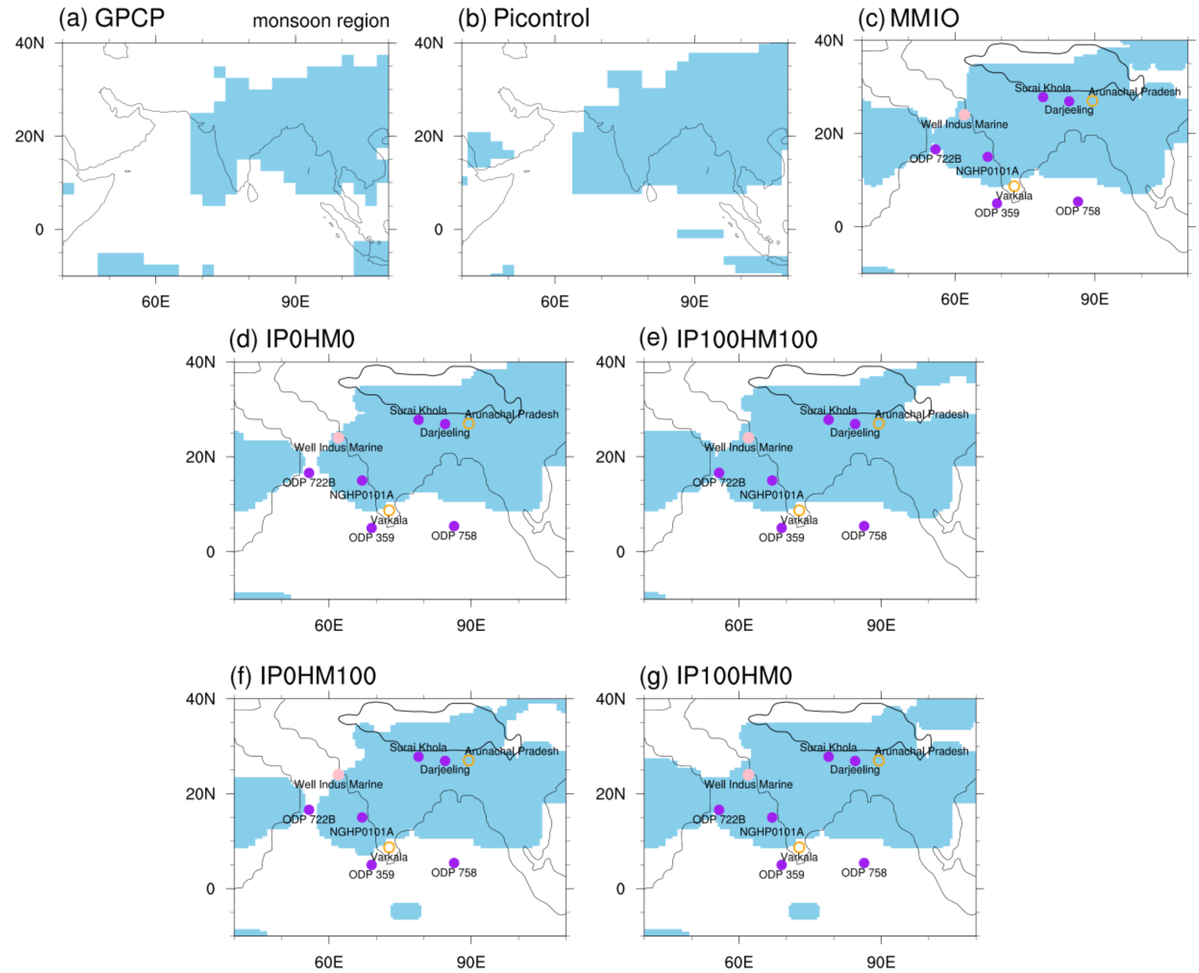

Figure 3. The monsoon domains (blue shading) in (a) GPCP, (b) piControl experiment, (c) MMIO experiment, (d) IP0HM0, (e) IP100HM100, (f) IP0HM100 and (g) IP100HM0 experiments, which are defined by the regions where local summer-minus-winter precipitation exceeds 2 mm day^{-1} and the local summer precipitation exceeds 55% of the annual total. Dots in (c-g) represent reconstructions near the SASM region, purple solid dots denote enhanced SASM, orange circles denote no significant change and pink solid dots denote weakened SASM from middle to late Miocene. The black contour in panel (c)-(g) indicates the altitude of 2500 m.

3.2. The effect of the HM and IP uplift

We first examine the effect of the joint uplift of the HM and IP (hereafter referred to as IP-HM). With the uplift of the IP-HM (Fig. 4a), a prominent cyclonic anomaly is built to the west of the IP with the intensified southwesterlies from Africa via the Arabian Sea into the northwestern India. Increased precipitation is found along the eastern flank of the cyclonic anomaly to the slopes of the western HM and northeastern IP. In the eastern part of the monsoon region, the enhanced precipitation occurs mainly along the southern edge of the HM while the leeward side features a remarkably decreased precipitation, indicating the rain shadow effect.

Corresponding to the summer precipitation change in response to IP-HM uplift, the domain of the SASM expands westward over the Arabian Sea and the Indian subcontinent (Figs. 3d-e). The western extension over land is about 65°E in the IP0HM0 experiment and reaches 60°E in the IP100HM100 experiment, indicating that the change of the SASM is significant in the northwest of the Indian subcontinent. Interestingly, monsoonal signal exists in the IP0HM0 experiment, an analogue to the "early Miocene", indicating that proto-monsoon exists by having TP only, which is also found in previous studies (Sarr et al., 2022). At the site of ODP 722B, monsoonal signal is absent in IP0HM0 (Fig.3d), but present in IP100HM80 (MMIO, Fig. 3c) and IP100HM0 (Fig. 3e) when the IP-HM is uplifted.

We further separate the effect of the IP and HM uplift. The climate response to IP uplift (IP100-IP0) is estimated as ((IP100HM0-IP0HM0)+(IP100HM100-IP0HM100))/2. Similarly, the effect of HM uplift HM100-HM0 is estimated as ((IP0HM100-IP0HM0)+(IP100HM100-IP100HM0))/2. The changes in precipitation and low-level circulation much resemble that attributing to the IP-HM uplift (Fig. 4a), indicating that by itself, the IP can sustain major parts of the precipitation changes except over the central-eastern HM. The easterly anomaly across the Indian subcontinent indicates that the westerly is blocked by elevated IP from north India, facilitating moisture convergence and rainfall increase over the northern Indian continent. As a result, the regional mean precipitation increases by 1.1 and 2.0 mm/day over the core (7-30°N, 65-95°E) and western regions (15-35°N, 50-75°E), respectively.

In contrast to the widespread effect of the IP on the SASM, the HM uplift only has a local effect (Fig. 4c), which is mostly confined to the HM and its close vicinity, and the change in low level circulation is noisy and weak. The precipitation strongly increases along the southern slope of the HM and dramatically decreases on its leeward side, resembling the changes in precipitation in the eastern region caused by the IP-HM uplift. As a result, there is little change in the regional mean precipitation over the core and eastern regions (15-35°N, 75-95°E). Specially, the changes in precipitation patterns and low-level circulation between IP100HM100 and MMIO (not shown) closely resemble that shown in Fig. 4c, albeit with reduced intensity, indicating that further uplift of HM above the TP does not result in intensified SASM.

In summary, the joint influences of the IP-HM uplift on the SASM are the superimposed effect of the IP and HM. In the western region, i.e., from the Arabian Sea to the northwestern India and Pakistan, the IP plays a dominant role while in the eastern region, i.e., the east part of South Asia, the changes in the SASM mainly attribute to the HM uplift. And the western extension of the SASM domain over the Arabian Sea and the Indian subcontinent is mainly caused by the uplift of IP rather than HM (Figs. 3f-g).

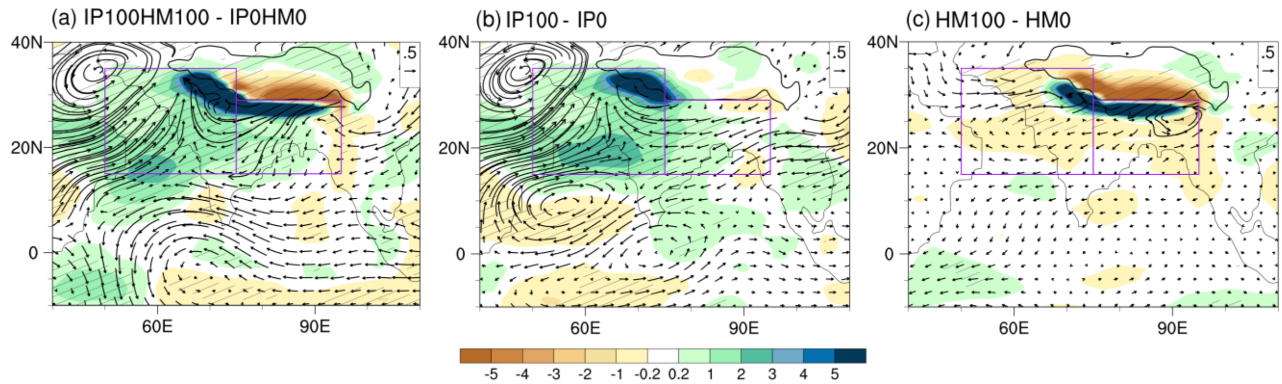

Figure 4. Precipitation (shaded, mm day^{-1}) and 850hPa wind differences between (a) IP100HM100 and IP0HM0 experiments; (b) IP100 and IP0 experiments; (c) HM100 and HM0 experiments. Here IP100-IP0=((IP100HM0-IP0HM0)+(IP100HM100-IP0HM100))/2, HM100-HM0=((IP0HM100-IP0HM0)+(IP100HM100-IP100HM0))/2. The black contour in each panel indicates the altitude of 2500 m. Purple boxes represent west (15-35°N, 50-75°E) and east (15-29°N, 75-95°E) parts of the South Asian monsoon region. Slashes indicate values >95% confidence level based on the *Student's t* test.

3.3. The effects of the CO_2 forcing vs topographic forcing

To illustrate the effect of CO2 forcing on SASM during the MMIO, we show the climatology of the SASM at low and high levels of CO_2 concentration based on MMIO28 and MMIO1000 experiments, respectively (Fig.5). The spatial circulation patterns in these two experiments are similar to that in the MMIO but the magnitudes change significantly (Fig.5a and b, Fig.2c). With the increase of CO_2, the meridional cross-equatorial flow slightly strengthens along the East Africa coast until 15°N but weakens to its east (Fig. 5c, d), leading to little change in the regional mean strength of this flow over the Arabian Sea. Meanwhile, precipitation enhances along the band of 15-25°N but decreases to its south, indicating a northward shift of the tropical rainfall belt. As the CO_2 rises from 280 ppm to 400 ppm, and subsequently to 1000 ppm, the AIR index correspondingly increases by 0.5 mm day^{-1} and 1.2

mm day^{-1}, respectively. MBA (SM2) further reveals that the increased monsoonal precipitation is primarily induced by enhanced thermodynamic conditions due to atmospheric warming, while the contribution from the change in large-scale monsoon circulation plays a secondary role (SM Fig S5c and d). For instance, the precipitation change between MMIO1000 and MMIO in the core SASM region is 1.2mm/day, of which 0.6 is from the thermodynamical processes related to changes in moisture and 0.25 mm/day from the dynamical processes related to circulation change.

To compare the effect of CO_2 forcing versus topographic forcing on the SASM, we examine the changes of precipitation and low-level circulations between MMIO1000 and IP0HM0 experiments (Fig. 5e), which actually reflects the combined effects of the CO_2 forcing (MMIO1000-MMIO) and IP-HM uplift (MMIO-IP0HM0). It is clear that the SASM changes in Fig. 5e bear the features of Fig. 5d and Fig. 4a: precipitation enhancing along the band of 15-25°N and reducing to its south in response to increased CO_2 and a prominent cyclonic anomaly built to the west of the IP in response to the IP-HM uplift. Moisture budget analysis further reveals that the enhanced precipitation of 3.2 mm day^{-1} in the west part of the SAM region is equally attributed to the vertical and horizontal moisture advection of 2.3 mm day^{-1} (Fig. 6). The moisture advection by anomalous meridional winds is the dominant contribution term, which is actually the response to the IP uplift as we see in next section.

We further examine the impacts of CO_2 forcing and topographic forcing in terms of WYI, SMJ, AIR (Sect. 2.4) and the mean precipitation over the western part of the SASM region (Fig.7). Under the topographic forcing, WYI exhibits small changes, with the exception of a relatively lower value in the IP0HM100 experiment. Concurrently, both precipitation and low-level circulation indices increase in response to the IP uplift, indicating a quasi-circulation-rainfall coupling relationship. With the increasing of CO_2 forcing, there is a noticeable decrease in WYI, whereas AIR and precipitation in the western SAM region increase significantly, indicating a decoupling relationship between large-scale circulation and monsoonal rainfall. The cross-equator flow at lower level (Somali Jet) is insensitive to CO_2 change as already shown in Fig.5.

The maximum difference of each index across the set of CO_2 or topographic sensitivity experiments is defined as the effect of each driver. In terms of WYI (Fig. 7a), the effect of CO_2 forcing is ~150% greater than that of IP-HM forcing, with values of 2.5 m s^{-1} vs 1.0 m s^{-1}. According to the AIR, the influence of CO_2 forcing is ~1.5 mm day^{-1}, which is comparable to that of IP-HM forcing (~1.5 mm day^{-1}) but is larger than the individual contributions of IP forcing (~1.0 mm day^{-1}) and HM forcing (~0.5 mm day^{-1}). In the western region, the effect of CO_2 forcing is about 75% compared to that of IP forcing (~1.5 vs ~2.0 mm day^{-1}). In summary, CO_2 forcing is the dominant driver for large-scale monsoon circulation, while the uplift of the IP exerts a more significant effect on regional circulation and the associated precipitation.

We note that the SASM response to CO_2 forcing in the Middle Miocene is very similar to that of projecting future climate change. For instance, increased SASM precipitation occurring with decreased WYI is also projected under abrupt quadrupling of CO_2 (Kong et al., 2022). The low-level monsoon circulations are projected to slightly weaken, consistent with the little change in the intensity of low-level cross-equator flow in our Miocene simulations (Fig.5 and 6). Based on an analysis across 20 climate models, Endo and Kitoh (2014) concluded that in a warmer world, projected increase in SASM precipitation is mainly attributed to thermodynamic processes. This finding aligns with our MBA result (Fig.5). The similarity in the SASM response to changes in CO_2 implies the presence of a comparable physical mechanism operating during the two warm periods.

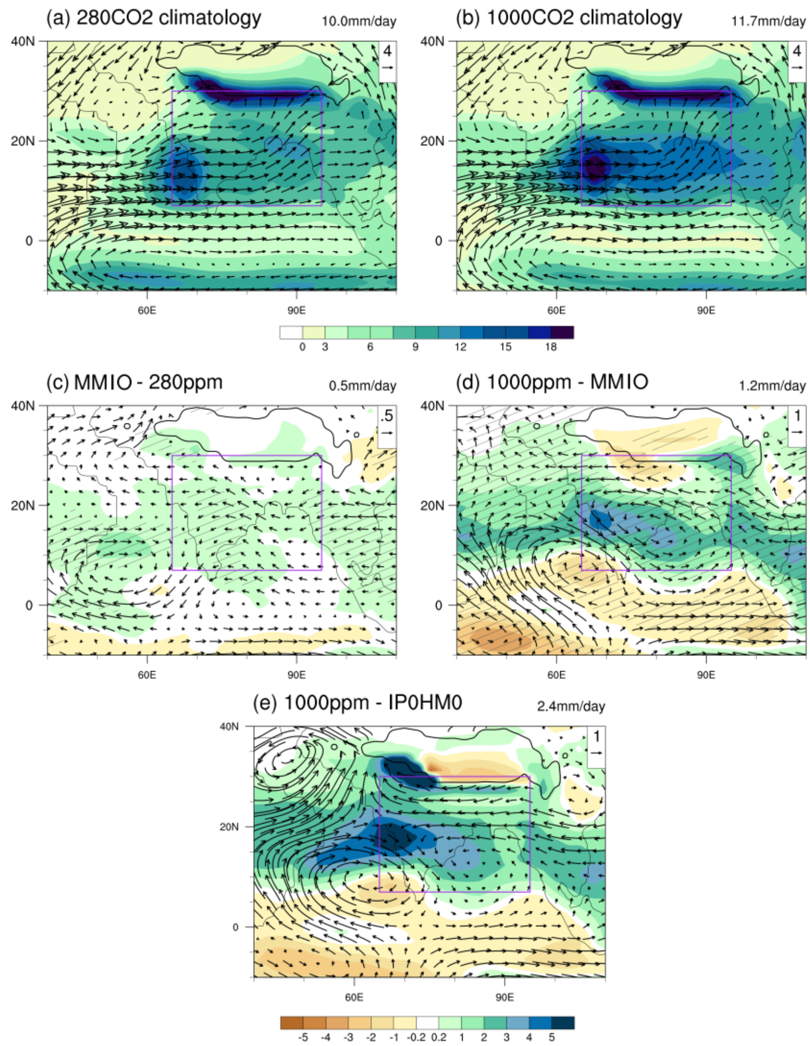

Figure 5. Climatology of JJA (June-July-August) mean South Asia summer monsoon (SASM) precipitation (mm day^{-1}) and 850 hPa winds (vectors, m s^{-1}) from (a) MMIO_280 experiments and (b) MMIO_1000 experiments. Precipitation (shaded, mm day^{-1}) and 850hPa wind differences (vector, m s^{-1}) between (c) MMCO and MMCO_280 experiments; (d) MMCO_1000 and MMCO experiments; (e)MMIO_1000 and IP0HM0 experiments.

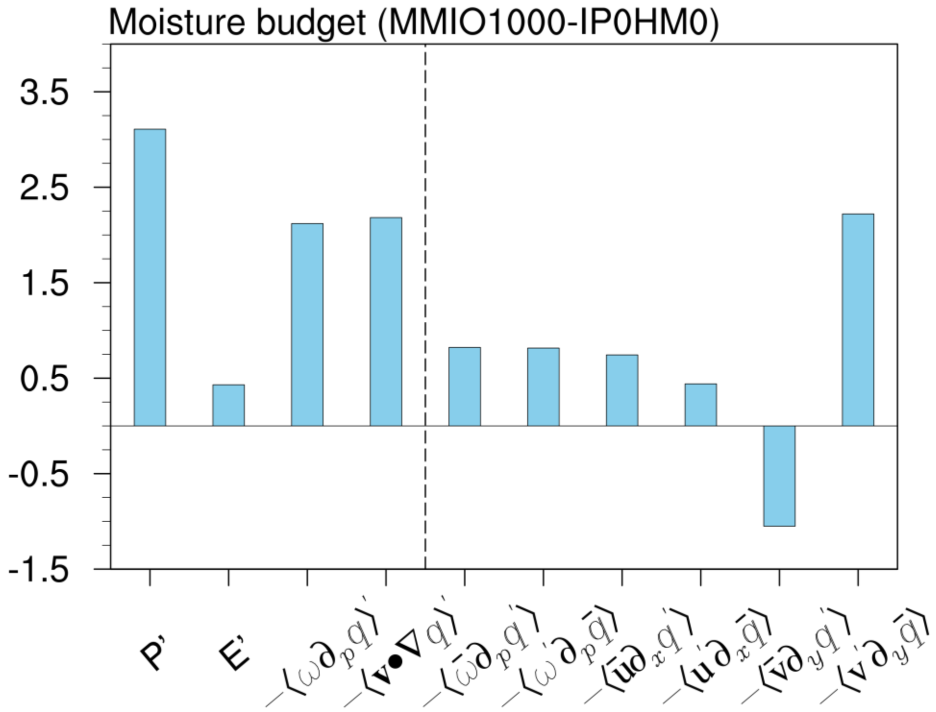

Figure 6. Moisture budget for regional mean precipitation differences (mm day^{-1}) over the west part (15-35°N, 50-75°E) of the South Asian monsoon region between MMIO1000ppm and IP0HM0 experiments.

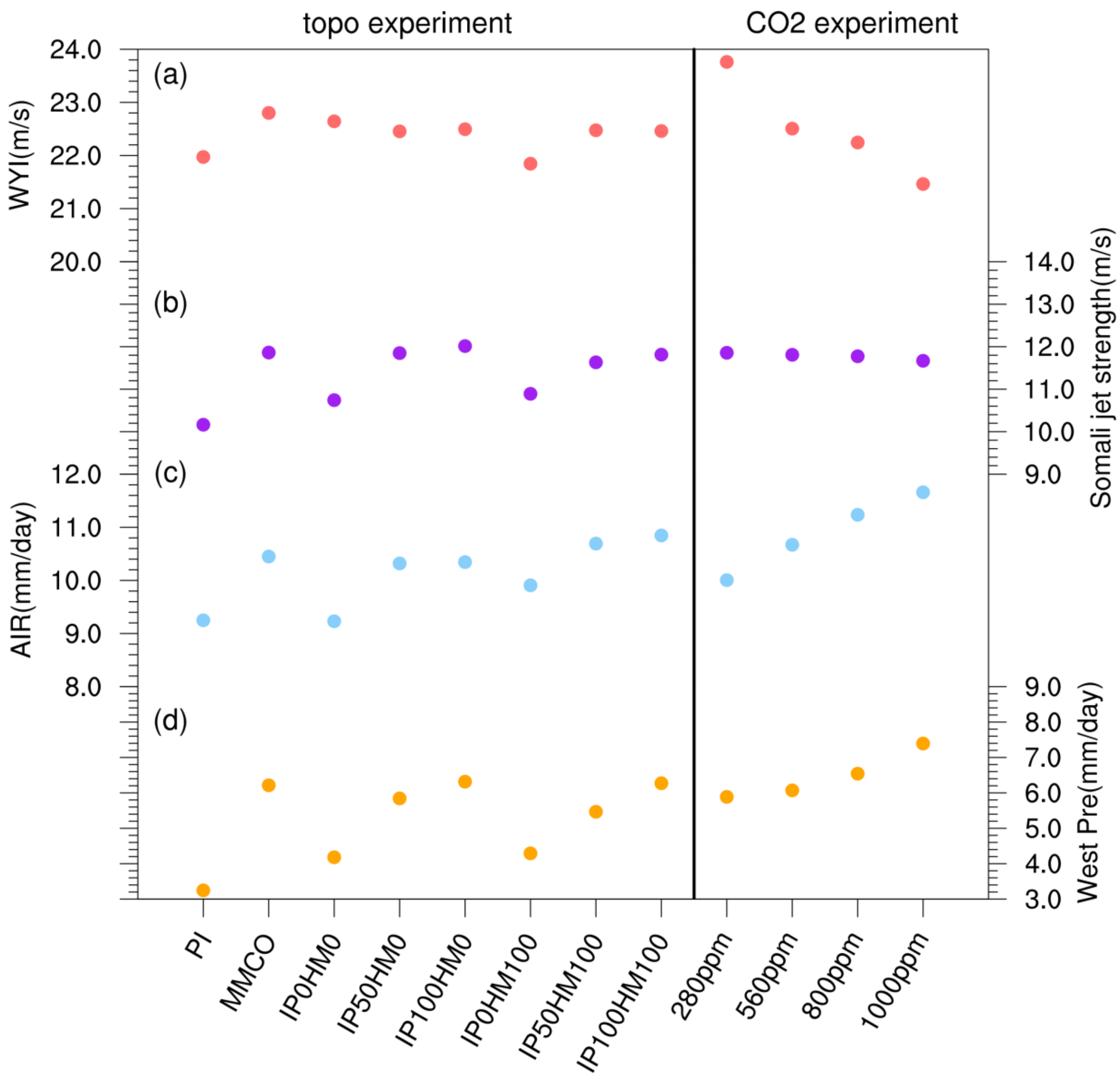

Figure 7. South Asian summer monsoon circulation and precipitation response in sensitivity experiments. Left, topography experiments. Right, CO_2 experiments. (a) Webster-Yang Index (meridional wind stress shear between 850 hPa and 200 hPa averaged over 40-110°E, 0-20°N during June-August). (b) Maximum intensity of the Somali jet over the Arabian Sea (averaged over 30-60°E, 0-20°N during June-August). (c) Regional mean precipitation over the land points within the domain (7-30°N, 65-95°E), named All indian rainfall (AIR). (d) Precipitation over the western part of South Asian summer monsoon region.

4. Mechanisms of the IP uplift on the SASM precipitation

To understand the mechanism of increased precipitation caused by IP uplift and HM uplift, we first use the moisture budget decomposition to identify the major moisture contributors. Here we provide the main analysis results (Fig.8), more details are seen in SM2. To focus our analyses on atmospheric dynamics, we neglect the contribution of evaporation, which is relatively small in our simulation despite the possibly important role for precipitation in the northwest India (Zhang et al., 2019). In response to IP uplift, the increased precipitation (2.0 mm day^{-1}) is largely attributed to the horizonal moisture advection (2.1 mm day^{-1}), in particular the moisture advection by anomalous meridional winds, while the vertical advection plays a secondary role (1.1 mm day^{-1}). In response to HM uplift, precipitation change (ca 1.2 mm day^{-1}) is mainly caused by the vertical moisture advection (0.9 mm day^{-1}) and is offset by the horizontal moisture advection (-0.4 mm day^{-1}). Its dominant contributor is a nonlinear term involving strong interaction between the vertical motion anomalies and moisture change (See SM2).

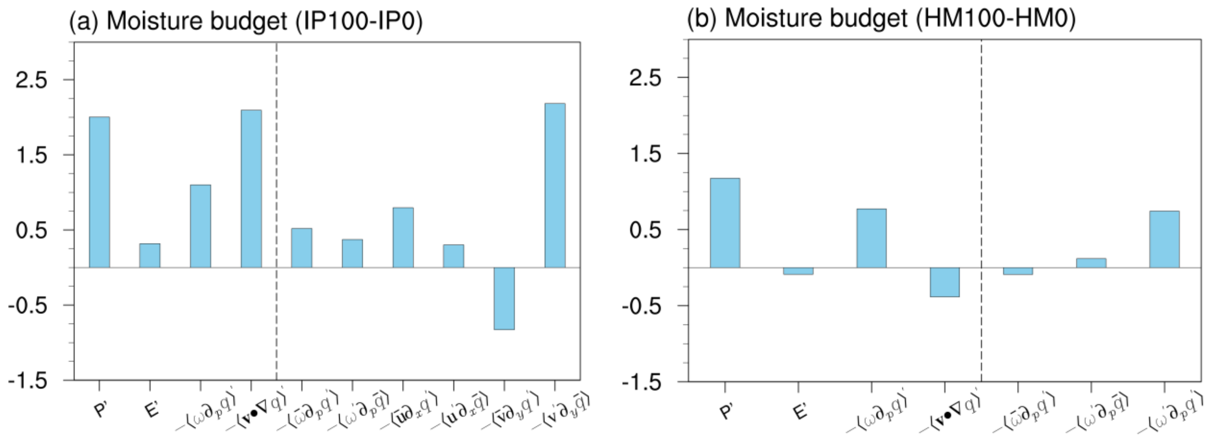

Figure 8. Moisture budget for regional mean precipitation differences (mm day^{-1}) over (a) the west part (15-35°N, 50-75°E) of the South Asian monsoon region between IP100 and IP0 experiments, (b) the east part (15-29°N, 75-95°E) of the South Asian monsoon region between HM100 and HM0 experiments.

We then examine the responses of the monsoon relevant variables to the uplifts of the IP and HM and the involved physical processes with focus on the effect of the IP. With IP uplift, the airs of high equivalent potential temperature (θ_e) at lower troposphere are accumulated in the IP and the surrounding region (Fig. 9a). The increased θ_e attributes to the enhancement of specific humidity (Fig. 9b) as moisture is advected by the anomalous southwesterly from North Africa via the Arabian Sea into the northwestern India and Pakistan (Fig. 9b), meanwhile it increases the convective instability. Triggered by surface sensible heating (Wu et al., 2012; Medina et al., 2010), convection takes place. At 500hPa, the upward motion anomalies are found over the IP and along the HM (Fig. 9c), reflecting the lifting effect of the elevated topography. The height of the lifted condensation level (LCL) is significantly reduced over the

IP and along the western edge of the HM (Fig. 9d), which is likely resulted from the elevated surface sensible heating (He, 2017). Reduced LCL facilitates the moist convection to occur, further warming the air parcels by the released latent heating. Consequently, specific humidity and θ_e further increase in the middle troposphere (Fig. 9e), which in return favors the convection activity. The pattern match between the specific humidity and θ_e indicates that the increased θ_e is primarily contributed by the increase of specific humidity then by the warming (Fig.9c). At the upper troposphere, forced by the latent heating, the warm-centered South Asian High strengthens over the IP (Fig. 9f), which is coupled with the cyclonic anomaly at low level (Fig. 9b), leading to moisture convergence over the western region and accelerate the convection activity. Positive feedback is thus built between precipitation and circulation. Regarding HM uplift, there is not a circulation adjustment between the low and high levels, the precipitation-circulation coupling thus cannot be built.

In this thermodynamical process, the IP's blocking/mechanical effect is also noticeable as it blocks the cold dry extratropical airs from northern India where the airs of high θ_e cumulate (Fig. 9a). However, this effect is relatively weak given the small contribution of the easterly anomaly to precipitation increase (less than 0.3 mm day^{-1}, see Fig. 8a: $-< u'\partial_x\overline{q} >$) according to the moisture budget.

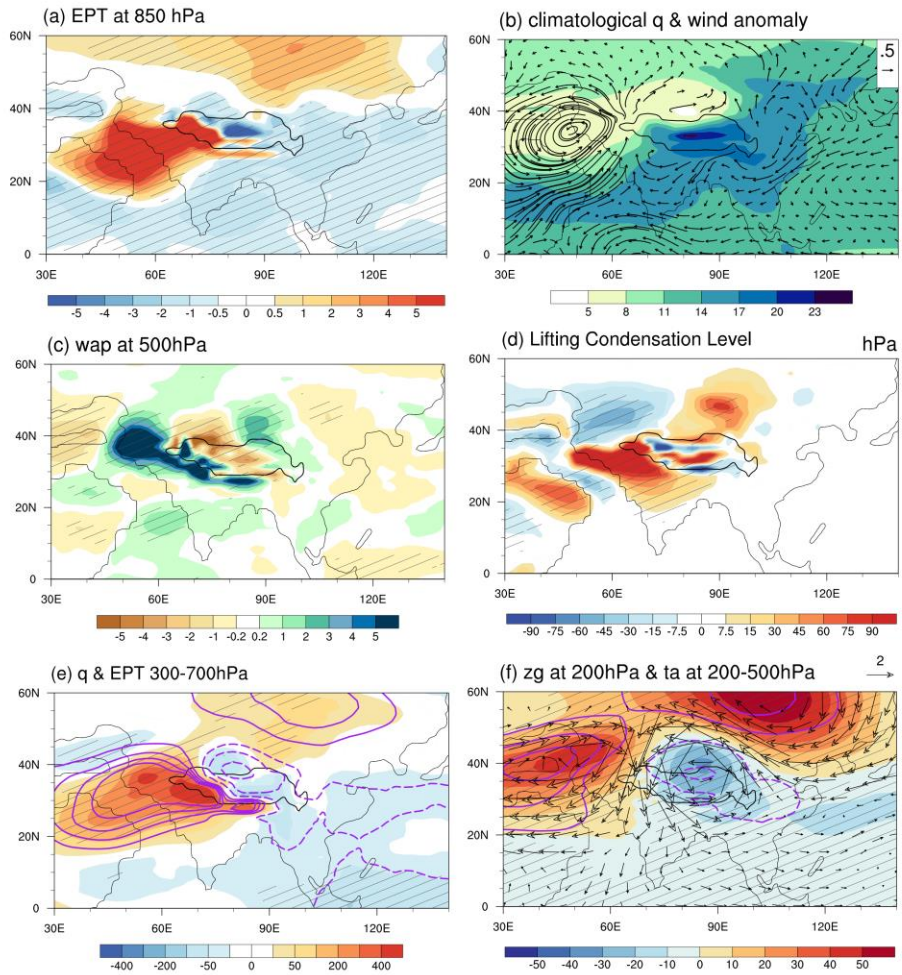

Figure 9. The differences of JJA mean thermal dynamical and dynamical variables between IP100HM100 and IP0HM0 simulations. (a) Equivalent Potential temperature (EPT, shading, unit: K) at 850 hPa; (b) climatological specific humidity q (shading, g/kg) and wind differences (vector, unit: m s^{-1}) at 850 hPa; (c) vertical velocity wap in pressure coordinate (-10^{-2} Pa/s) at 500 hPa; (d) Lifting condensation level (LCL, unit: hPa, positive value represents lower LCL); (e) Specific humidity (shading) and EPT (contours, unit: K) integrated between 300 and 700 hPa; (f) geopotential height zg (shading, unit: m), temperature anomalies (contours, unit: K) and wind (vector, unit: m s^{-1}) at 200 hPa.

5. Discussion

5.1. Application to monsoonal reconstructions

A remarkable intensification of the SASM in the Middle Miocene is revealed by increasing evidence (Fig. 3c; Table 2). In the western India and the Arabian Sea, monsoon-like precipitation appeared in the early Miocene (Clift et al., 2008; Reuter et al., 2013; Ali et al., 2021) and intensified at ~15-12 Ma (Clift et al., 2008; Yang et al., 2020). In the eastern India, the intensification of SASM occurred at ca 15 Ma (Khan et al., 2014) to ~13-11 Ma (Bhatia et al., 2021; Vogali et al., 2017). In terms of wind system, a weaker "proto-monsoon" existed between 25 and 12.9 Ma (Betzler et al., 2016) and an abrupt intensification occurred at 12.9 Ma inferred from the sedimentary records in the Maldives (Betzler et al., 2016) and in the western Arabian Sea (Gupta et al., 2015), indicating the inception of a modern Somali Jet. Besides, monsoonal upwelling thus possibly the strengthening of wind speed in the western Arabian Sea was observed since ca 14.8 Ma.

Our modeling results support the existence of the SASM (Clift et al., 2008) in terms of precipitation seasonality in early Miocene represented by the IP0HM0 experiment when the proto-TP existed while the IP and HM were low (Fig.3). With the uplift of the IP rather than the HM during middle Miocene, monsoonal precipitation increased in the northwest of the Indian landmass as shown in the ~IP50, ~HM50 and IP100HM100 experiments (Fig.6) corroborating the hypothesis that increased sedimentary and weathering fluxes between 25 and 15 Ma could be partially linked with monsoon intensification related to the coeval of IP-HM (Clift et al., 2008). Meanwhile, with the deepening of cyclonical anomaly over the west of the IP (Fig.4b), southwesterly strengthens in the western Arabian Sea, which somewhat agrees with the reconstructions that suggests the inception of modern Somali Jet (Betzler et al., 2016). But the inception of modern Somali Jet is more likely attributed to the uplift of the East African topography demonstrated in modeling studies (Chakraborty et al., 2006; Wei and Bordoni, 2016; Sarr et al., 2022; Tardif et al., 2023) and/or the emergence of land in Eastern Arabian Peninsula (Sarr et al., 2022). This aligns with geological evidence indicating that the East Africa began to uplift in the late Oligocene–early Miocene and rapidly uplifted in the middle–late Miocene (Macgregor, 2015). We conduct a series of complementary experiments (SM3) and confirm that elevated East African highlands play an essential role in producing the modern-like Somali Jet. Meanwhile, it creates an anti-cyclonic anomaly over the north Arabian Sea as revealed by previous studies, leading to reduced moisture transport into Indian landmass thus decreased monsoonal precipitation. Therefore, there is likely a complementary and competing effect on SASM evolution between the uplift of the IP and the East African highlands.

The enhanced precipitation at 13 Ma is inferred from leaf fossil in the eastern HM, which has been attributed to the rise of the HM (Khan et al., 2014; Bhatia et al., 2021). But this hypothesis cannot be supported by our sensitivity experiment. Neither can it be interpreted by the uplift of the IP based on our simulations. In contrast, some modeling studies suggested enhanced precipitation in along the HM in response to mountain uplift in the American region and northern TP (Chakraborty et al., 2006; Miao et al., 2022). Therefore, remote impacts on precipitation change in the eastern HM should be taken into account.

The CO_2 forcing has little impact on the intensity of the Somali Jet, indicating its little contribution to the strengthening of surface wind inferred from the reconstructions (Gupta et al., 2015), but its effect on precipitation is likely to superimpose on that of the IP uplift. It is speculated that during the early part of the Middle Miocene Climatic Optimum, abrupt rise of the CO_2 amplifies the effect of the IP uplift, leading to the markedly intensified SASM precipitation around 15 Ma as depicted in reconstructions (Clift et al., 2008; Yang et al., 2020). While during the mid-late Miocene, the decreasing tendency of CO_2 offsets the effect of the IP uplift, although precipitation still intensifies due to the dominant impact of the latter. Given the wide range of reconstructed CO_2 in terms of intensity and timing during the Middle Miocene, the effect of CO_2 forcing experiences large uncertainty. Nevertheless, the CO_2 variation itself cannot interpret the strengthening of wind along the Somali or the evolution of SASM precipitation intensity as inferred from the reconstructions.

The two sites ODP 359 and 758, situated in the Inner Sea of the Maldives and the southern Bay of Bengal, respectively, indicate an abrupt strengthening of monsoonal circulations in the SASM regions at 12.9 Ma and 13.9 Ma, respectively. However, our modeling efforts cannot replicate these enhancements through either the uplift of the IP and HM or a reduction in CO2 levels. Hence, it is likely that other factors exert a more significant influence on the reorganization of the SASM system. Examples include Antarctic glaciation, as suggested in Ali et al. (2021; Sarr et al., 2021), as well as the closure of the Tethys, as discussed in research by Betzler et al. (2016) and Bialik et al. (2019).

5.2. Comparison with previous modeling studies

Concerning the effect of uplifted HM and IP on the SASM, our modeling results confirm the intensified SASM linked with the uplift of the IP (Liu et al., 2017; Zhang et al., 2015; Acosta and Huber, 2020; Tardif et al., 2020, 2023) rather than the HM (Zhang et al., 2012), particularly over the western region, i.e., from the Arabian Sea to the northwestern India and Pakistan. When the evolution history of the HM-TP is taken into account, the uplift of the HM against the TP mainly enhances the orographic precipitation along the windward side of the HM and has little impact on regional monsoonal precipitation. While the effects of IP uplift from our AOCGM simulations qualitatively agree with previous studies using AGCMs (Wu et al., 2012; Liu et al., 2017; Zhang et al., 2015; Acosta and Huber, 2020), additional analysis (not shown) reveals notable impacts on ocean circulations. These impacts are evidenced by changes in SSTs and precipitation in tropical oceans, potentially influencing SASM intensity through teleconnection. However, further discussion on the added value of OAGCM extends beyond the scope of our current study.

Regarding the mechanism of the IP uplift on the SASM, our analyses tend to support its thermal forcing effect (Wu et al., 2012; Liu et al., 2017), but instead of emphasizing the sensible heating effect, we highlight the latent heating as a crucial link between the convection activity and regional circulations as previous study (He, 2017). This demonstrates that it is not only temperature, but also the hydrological cycle modifications as depicted in Section 4 must be taken into account to understand the involved physical process. We also note that the IP's blocking/mechanical effect is much weaker in our study than that reported in Tang et al. (2013). In their study, the elevated IP effectively blocked the westerly flow to the south of the HM, facilitating the moisture advection from the Bay of Bengal into northern India, thus strongly enhanced the SASM precipitation, particularly in eastern India. Similar blocking effect (or role of gatekeeper) is also reported by Acosta and Huber (2020). Both studies utilized high spatial resolution models and were conducted using modern geographies. The weak blocking effect in our study is likely due to: (1) smaller size of the IP in the Miocene than in the present day; (2) spatial lower-resolution model than that used in their studies (~1° or higher), thus some critical regional circulations linked to the SASM are likely misrepresented (Boos and Hurley, 2013; Acosta and Huber, 2017).

5.3. Uncertainty and Methodological Limitation

Geography, particularly the land-sea distribution, is another important driver for Asian monsoon development (Ramstein et al., 1997; Farnsworth et al., 2019; Sarr et al., 2022; Tardif et al., 2023). The land-sea distribution used in our Miocene simulations, like other reconstructions (Herold et al., 2008; He et al., 2021, and references therein) inevitably contain uncertainties. For instance, the Bohai Bay and Yellow Sea basins in East Asia are open in the F18, contrary to regional stratigraphy and lithofacies records (Tan et al., 2020). The Greenland-Scotland Ridge in F18 is set as ~4000 m, significantly deeper than a middle bathyal environment (<1000-m deep) indicated by geological evidence (Stocker et al., 2005). Large uncertainties also present in the Tethys/Paratethys configuration. The Tethyan Seaway is open with a depth of over 3000 m in F18, in contrast to geological evidence suggesting intermittent openings during ~15-12.8 Ma (Sun et al., 2021). The Paratethys was intermittently connected and disconnected from the global ocean during the Middle Miocene according to geological studies (Rögl, 1997). It is assigned to connect to the global ocean in F18 and Herold et al. (2008) while it retreats to the Carpathian-Black Sea-Caspian Sea region and is connected with the Mediterranean in He et al. (2021). In short, the Tethys/Paratethys configuration in F18 reflects more the feature of early Middle Miocene geography, with an open Tethyan Seaway and a smaller IP. However, given that most reconstruction records focus on the late Middle Miocene period (14-12 Ma), our Middle Miocene simulations may not adequately capture the IP's effects and may be less suitable for comparison with proxy data. Nonetheless, a previous study (Sarr et al., 2022) utilizing a late Miocene (10 Ma) configuration also emphasized the significant role of the Anatolia–Iran uplift on enhanced SASM. Their experiments showed that this uplift deepened the low-pressure area over the Arabian Peninsula, intensifying low-level wind and moisture transport from the Arabian Sea towards South Asia, a process consistent with our simulations (Fig. 4a). We thus emphasize that constraining the exact timing of IP uplift is crucial to improve our understanding of the evolution of the SAM. During the late Middle Miocene period, significant geological events occurred, including the final closure of the Tethyan Seaway ~14 Ma (Sun et al., 2021) and the remarkable expansion of the Antarctic ice sheets from ~14.2 to 13.8 Ma (Holbourn et al., 2005), resulting in global sea-level changes. These geological events likely led to considerable changes in the physiography of the Middle East and East Africa. Consequently, the atmospheric and oceanic circulations in these regions and beyond are likely altered during the late Middle Miocene (Hamon et al., 2013). But some modelling studies indicated that "the sole effect of the Tethys way closure, without strong modification of land extension in the Arabian Peninsula region, remain limited" (Tardif et al., 2023), thereby not supporting the hypothesis that the closure of the Tethys Seaway may contribute to altering the intensity of the monsoon during the Miocene (Bialik et al., 2020; Sun et al., 2021).

The uncertainty regarding the effects of CO_2 on SASM primarily arises from the wide range of estimated CO_2 values during the Middle Miocene. While our CO_2 sensitivity experiments cover various concentrations, prior studies (Thomson et al., 2021) indicate that the impacts of CO_2 variation on SASM are influenced by the background state. For instance, the status of the Tethys Sea, whether open or closed, introduces uncertain changes in SASM rainfall. Consequently, understanding the precise impacts of CO_2 variation on SASM behavior remains complex and warrants further investigation. In brief, the evolution of the SASM during the Middle Miocene could have been caused by a combination of changes in topography in East

African and Middle Eastern physiography, CO_2 variation, as well as the progressive cryosphere expansion in Antarctica. All these factors should be addressed in future study with careful experimental design.

High-resolution model is essential to capturing the monsoon dynamics and thermodynamics thus improves our understanding of the monsoonal variation/change (Acosta and Huber, 2017; Anand et al., 2018; Botsyun et al., 2022a, b). The climate model employed in present study is a version of low spatial resolution, not sufficient to reproduce the regional features of the SASM. For instance, the Indo-Gangetic low-level jet, a key mechanism that introduces monsoon onshore flow from the Bay of Bangla into northern India (Acosta and Huber, 2017), is missing in our modern simulation as all the low-resolution models do. Misrepresentation of this circulation is problematic for interpreting the effect of HM uplift and reconciling the modeling-proxy data discrepancy (Khan et al., 2014; Vogeli et al., 2017; Bhatia et al., 2021). The low resolution also likely underestimates the barrier effect of the IP due to topography smooth (Boos and Hurley, 2013). For instance, the mechanical blocking effect is more prominent in the studies with high-resolution models (Tang et al., 2013; Acosta and Huber, 2020) than those with coarse resolution model (Zhang et al., 2015; Wu et al., 2007). Although it is out of computer resources to run coupled paleoclimate simulations and perform many sensitivity experiments with high resolution version, we acknowledge that a better understanding of the impact of topographic change on the SASM and the underlying mechanism would benefit from additional simulations performed with increased spatial resolution.

The evolution of the SASM is also largely determined by large scale circulation (Wu et. al., 2012; Botsyun et al., 2022b). For instance, the mid-latitude westerly Jet migrated earlier (in the year) and reached higher latitude during warm climate periods than in the pre-industry (Botsyun et al., 2022b). Our Miocene experiments likely confirm this point (not shown) but investigation in depth needs to be done in the future. We also acknowledge that running OAGCMs necessitates an extended period to achieve equilibrium. Particularly with significant modifications to topography or CO_2 levels, integrations spanning 200/500 years may carry the risk of non-equilibrium, potentially affecting the quantitative estimation of their effects, but not essentially change the results.

6. Conclusions

In this study, we performed a series of 12 experiments with the fully coupled OAGCM CESM1.2 (with ~2° horizontal resolution) to investigate the SASM in response to topographic changes in the region surrounding the Tibetan Plateau and the variations of global CO_2 concentration during the Middle Miocene. We examined the effect of elevated IP and HM on the SASM through a set of topographic sensitivity experiments. Additionally, due to the large uncertainties of CO_2 reconstructions (Rae et al., 2021; CenCO_2PIP, 2023), we conducted a series of CO_2 sensitivity experiments to investigate its impact on the SASM. We explored the underlying mechanisms and compare the modeling results with proxy data. The conclusions are as follows:

(1) We confirm and extend previous studies showing that IP uplift plays a major role in the intensification of the SASM, particularly in the western region, from the northern Arabian Sea to northwestern India and Pakistan, while it has little impact on eastern India. The effect of the HM uplift is confined to the range of the HM and its vicinity, producing orographic precipitation change.

(2) The response of the SASM to CO_2 variation under Middle Miocene boundary conditions is similar to that under present-day conditions projecting future SASM changes. This suggests that similar physical processes operate during these two warm periods. Enhanced monsoonal precipitation is primarily governed by enhanced thermodynamic conditions due to atmospheric warming, while the contribution from the change in large-scale monsoon circulation plays a secondary role. In the western region, topographic change, particular the IP uplift, remain the dominant factor.

(3) Topographic changes out-compete CO_2 variations in driving the intensification of the SASM. The forcing of CO_2 variation is more important for the change of large-scale monsoon circulation that is decoupled with rainfall change. In case of strong CO_2 variation, that is, from 280 to 1000 ppm, similar to the abrupt-3× or 4× CO_2 experiments, its contribution to SASM precipitation is comparable (approximately 75%~100%) to that of topographic forcing in the core SAM region. However, in the western region, topographic forcing remains the dominant factor.

(4) We propose a thermodynamic process linking the uplift of the IP to enhanced SASM, where a deepened thermal low transports moisture from the Arabian Sea to the western region, coupled with the South Asian High linked by latent heat release. However, the strong thermal effect of the uplifted IP in our Middle Miocene simulation is possibly associated with the

smaller size of the IP and model's low-resolution, which tends to underestimate the mechanical effects.

(5) Compared with reconstructions, the effect of IP uplift is in good agreement with observed evolution of precipitation and the change of wind intensity while the effects of the HM uplift and CO_2 variation are insufficient to interpret the proxies.

Code availability

The data in this study were analyzed and the figures were created with NCAR Command Language. All relevant codes used in this work are available, upon request, from the corresponding author Y.Z.

Data availability

The processed model outputs used to reproduce the figures in this manuscript are archived at a Zenodo repository: https://doi.org/10.5281/zenodo.12201243 (Zuo et al., 2024). Instructions and permissions to relevant experiments will be provided upon request to Y.Z. Source code of CESM1.2 can be downloaded from https://www2.cesm.ucar.edu/models/cesm1.2/.

Author contribution

MZ and YZ wrote the draft manuscript and analyzed the simulations. YS performed the simulations; GR and TZ modified the draft and particularly corrected the abstract and conclusions. YZ and DL conceived and developed the research. All authors participated in the final version of the manuscript.

Competing interest

The authors declare that they have no conflict of interest.

Acknowledgements

This work is jointly supported by the National Natural Science Foundation of China (Grants 41988101, 42105047) and the Second Tibetan Plateau Scientific Expedition and Research Program (STEP; Grant No. 2019QZKK0708). Model simulations presented in this study were performed on the supercomputer of Chinese Academy of Science Jin Cloud.

References

Acosta, R. P., and M. Huber, 2017: The neglected Indo-Gangetic plains low-level jet and its importance for moisture transport and precipitation during the peak summer monsoon. Geophysical Research Letters, 44, 8601-8610, https://doi.org/10.1002/2017gl074440.

Acosta, R.P., Huber, M., 2020. Competing Topographic Mechanisms for the Summer Indo-Asian Monsoon. Geophysical Research Letters 47, e2019GL085112. https://doi.org/10.1029/2019GL085112

Agard, P., Omrani, J., Jolivet, L., Whitechurch, H., Vrielynck, B., Spakman, W., Monié, P., Meyer, B., Wortel, R., 2011. Zagros orogeny: a subduction-dominated process. Geological Magazine 148, 692–725. https://doi.org/10.1017/S001675681100046X

Ali, S., E. C. Hathorne, and M. Frank, 2021: Persistent provenance of south asian monsoon-induced silicate weathering over the past 27 million years. Paleoceanography and Paleoclimatology, 36, https://doi.org/10.1029/2020pa003909.

Anand, A., Mishra, S.K., Sahany, S., Bhowmick, M., Rawat, J.S., Dash, S.K., 2018. Indian Summer Monsoon Simulations: Usefulness of Increasing Horizontal Resolution, Manual Tuning, and Semi-Automatic Tuning in Reducing Present-Day Model Biases. Sci Rep 8, 3522. https://doi.org/10.1038/s41598-018-21865-1

An, Z. S., J. E. Kutzbach, W. L. Prell, and S. C. Porter, 2001: Evolution of asian monsoons and phased uplift of the himalayan tibetan plateau since late miocene times. Nature, 411, 62-66, https://doi.org/10.1038/35075035.

Ballato, P., Cifelli, F., Heidarzadeh, G., Ghassemi, M.R., Wickert, A.D., Hassanzadeh, J., Dupont-Nivet, G., Balling, P., Sudo, M., Zeilinger, G., Schmitt, A.K., Mattei, M., Strecker, M.R., 2017. Tectono-sedimentary evolution of the northern Iranian Plateau: insights from middle–late Miocene foreland-basin deposits. Basin Research 29, 417–446. https://doi.org/10.1111/bre.12180

Betzler, C., and Coauthors, 2016: The abrupt onset of the modern south asian monsoon winds. Sci. Rep., 6, https://doi.org/10.1038/srep29838.

Bhatia, H., Srivastava, G., Spicer, R.A., Farnsworth, A., Spicer, T.E.V., Mehrotra, R.C., Paudayal, K.N., Valdes, P., 2021. Leaf physiognomy records the Miocene intensification of the South Asia Monsoon. Global and Planetary Change 196, 103365. https://doi.org/10.1016/j.gloplacha.2020.103365

Bialik, O. M., G. Auer, N. O. Ogawa, D. Kroon, N. D. Waldmann, and N. Ohkouchi, 2020: Monsoons, upwelling, and the deoxygenation of the northwestern indian ocean in response to middle to late miocene global climatic shifts. Paleoceanography and Paleoclimatology, 35, https://doi.org/10.1029/2019pa003762.

Boos, W., Kuang, Z., 2010. Dominant control of the South Asian Monsoon by orographic insulation versus plateau heating. Nature 463, 218–22. https://doi.org/10.1038/nature08707

Boos, W.R., Hurley, J.V., 2013. Thermodynamic Bias in the Multimodel Mean Boreal Summer Monsoon. Journal of Climate 26, 2279–2287. https://doi.org/10.1175/JCLI-D-12-00493.1

Botsyun, S., Ehlers, T.A., Koptev, A., Böhme, M., Methner, K., Risi, C., Stepanek, C., Mutz, S.G., Werner, M., Boateng, D., Mulch, A., 2022a. Middle Miocene Climate and Stable Oxygen Isotopes in Europe Based on Numerical Modeling. Paleoceanography and Paleoclimatology 37, e2022PA004442. https://doi.org/10.1029/2022PA004442

Botsyun, S., Mutz, S.G., Ehlers, T.A., Koptev, A., Wang, X., Schmidt, B., Appel, E., Scherer, D.E., 2022b. Influence of Large-Scale Atmospheric Dynamics on Precipitation Seasonality of the Tibetan Plateau and Central Asia in Cold and Warm Climates During the Late Cenozoic. Journal of Geophysical Research: Atmospheres 127, e2021JD035810. https://doi.org/10.1029/2021JD035810

Burls, N.J., Bradshaw, C.D., Boer, A.M.D., Herold, N., Huber, M., Pound, M., Donnadieu, Y., Farnsworth, A., Frigola, A., Gasson, E., Heydt, A.S. von der, Hutchinson, D.K., Knorr, G., Lawrence, K.T., Lear, C.H., Li, X., Lohmann, G., Lunt, D.J., Marzocchi, A., Prange, M., Riihimaki, C.A., Sarr, A.-C., Siler, N., Zhang, Z., 2021. Simulating Miocene Warmth: Insights From an Opportunistic Multi-Model Ensemble (MioMIP1). Paleoceanography and Paleoclimatology 36, e2020PA004054. https://doi.org/10.1029/2020PA004054

Chakraborty, A., Nanjundiah, R.S., Srinivasan, J., 2006. Theoretical aspects of the onset of Indian summer monsoon from perturbed orography simulations in a GCM. Annales Geophysicae 24, 2075–2089.

Chen, G.-S., Liu, Z., Kutzbach, J., 2014. Reexamining the barrier effect of the Tibetan Plateau on the South Asian summer monsoon. Climate of the Past 10. https://doi.org/10.5194/cp-10-1269-2014

Chou, C., J. D. Neelin, C.-A. Chen, and J.-Y. Tu, 2009: Evaluating the "rich-get-richer" mechanism in tropical precipitation change under global warming. J. Climate, 22, 1982-2005, https://doi.org/10.1175/2008jcli2471.1.

Clift, P.D., Hodges, K.V., Heslop, D., Hannigan, R., Van Long, H., Calves, G., 2008. Correlation of Himalayan exhumation rates and Asian monsoon intensity. Nature Geosci 1, 875–880. https://doi.org/10.1038/ngeo351

Clift, P.D., Webb, A.A.G., 2019. A history of the Asian monsoon and its interactions with solid Earth tectonics in Cenozoic South Asia. Geological Society, London, Special Publications 483, 631–652. https://doi.org/10.1144/SP483.1

Ding, L., Spicer, R.A., Yang, J., Xu, Q., Cai, F., Li, S., Lai, Q., Wang, H., Spicer, T.E.V., Yue, Y., Shukla, A., Srivastava, G., Khan, M.A., Bera, S., Mehrotra, R., 2017. Quantifying the rise of the Himalaya orogen and implications for the South Asian monsoon. Geology 45, 215–218. https://doi.org/10.1130/G38583.1

Ding, L., P. Kapp, F. Cai, C. N. Garzione, Z. Xiong, H. Wang, and C. Wang, 2022: Timing and mechanisms of tibetan plateau uplift. Nature Reviews Earth & Environment, https://doi.org/10.1038/s43017-022-00318-4.

Endo, H., and A. Kitoh, 2014: Thermodynamic and dynamic effects on regional monsoon rainfall changes in a warmer climate. Geophysical Research Letters, 41, 1704-1710, https://doi.org/10.1002/2013gl059158.

Eyring, V., Bony, S., Meehl, G.A., Senior, C.A., Stevens, B., Stouffer, R.J., Taylor, K.E., 2016. Overview of the Coupled Model Intercomparison Project Phase 6 (CMIP6) experimental design and organization. Geoscientific Model Development 9, 1937–1958. https://doi.org/10.5194/gmd-9-1937-2016

Farnsworth, A., Lunt, D.J., Robinson, S.A., Valdes, P.J., Roberts, W.H.G., Clift, P.D., Markwick, P., Su, T., Wrobel, N., Bragg, F., Kelland, S.-J., Pancost, R.D., 2019. Past East Asian monsoon evolution controlled by paleogeography, not CO2. Science Advances 5, eaax1697. https://doi.org/10.1126/sciadv.aax1697

Fluteau, F., Ramstein, G., Besse, J., 1999. Simulating the evolution of the Asian and African monsoons during the past 30 Myr using an atmospheric general circulation model. Journal of Geophysical Research: Atmospheres 104, 11995–12018. https://doi.org/10.1029/1999JD900048

Frigola, A., Prange, M., Schulz, M., 2018. Boundary conditions for the Middle Miocene Climate Transition (MMCT v1. 0). Geoscientific Model Development 11, 1607–1626.

Gent, P.R., Danabasoglu, G., Donner, L.J., Holland, M.M., Hunke, E.C., Jayne, S.R., Lawrence, D.M., Neale, R.B., Rasch, P.J., Vertenstein, M., Worley, P.H., Yang, Z.-L., Zhang, M., 2011. The Community Climate System Model Version 4. Journal of Climate 24, 4973–4991. https://doi.org/10.1175/2011JCLI4083.1

Goldner, A., Herold, N., Huber, M., 2014. The Challenge of Simulating the Warmth of the Mid-

Miocene Climatic Optimun in CESM1. Climate of the Past.

Gupta, A. K., A. Yuvaraja, M. Prakasam, S. C. Clemens, and A. Velu, 2015: Evolution of the south asian monsoon wind system since the late middle miocene. Palaeogeography Palaeoclimatology Palaeoecology, 438, 160-167, https://doi.org/10.1016/j.palaeo.2015.08.006.

Hamon, N., Sepulchre, P., Lefebvre, V., Ramstein, G., 2013. The role of eastern Tethys seaway closure in the Middle Miocene Climatic Transition (ca. 14 Ma). Climate of the Past 9, 2687–2702. https://doi.org/10.5194/cp-9-2687-2013

Harris, N., 2006. The elevation history of the Tibetan Plateau and its implications for the Asian monsoon. Palaeogeography, Palaeoclimatology, Palaeoecology, Monsoon and Tectonics of Asia 241, 4–15. https://doi.org/10.1016/j.palaeo.2006.07.009

He, B., 2017. Influences of elevated heating effect by the Himalaya on the changes in Asian summer monsoon. Theor Appl Climatol 128, 905–917. https://doi.org/10.1007/s00704-016-1746-5

He, Z., Zhang, Z., Guo, Z., Scotese, C.R., Deng, C., 2021. Middle Miocene (∼14 Ma) and Late Miocene (∼6 Ma) Paleogeographic Boundary Conditions. Paleoceanography and Paleoclimatology 36, e2021PA004298. https://doi.org/10.1029/2021PA004298

Herold, N., M. Huber, and R. D. Mueller, 2011: Modeling the miocene climatic optimum. Part i: Land and atmosphere. J. Climate, 24, 6353-6372, https://doi.org/10.1175/2011jcli4035.1.

Herold, N., Seton, M., Müller, R.D., You, Y., Huber, M., 2008. Middle Miocene tectonic boundary conditions for use in climate models. Geochemistry, Geophysics, Geosystems 9.

Hersbach, H., and Coauthors, 2020: The era5 global reanalysis. Quarterly Journal of the Royal Meteorological Society, 146, 1999-2049, https://doi.org/10.1002/qj.3803.

Holbourn, A., Kuhnt, W., Schulz, M., Erlenkeuser, H., 2005. Impacts of orbital forcing and atmospheric carbon dioxide on Miocene ice-sheet expansion. Nature 438, 483–487. https://doi.org/10.1038/nature04123

Huffman, G. J., R. F. Adler, D. T. Bolvin, and G. Gu, 2009: Improving the global precipitation record: Gpcp version 2.1. Geophys. Res. Lett., 36, https://doi.org/10.1029/2009gl040000.

Hunke, E.C., Lipscomb, W.H., 2010. CICE: the Los Alamos Sea Ice Model Documentation and Software User’s Manual Version 4. 1–76.

Jin, C., B. Wang, and J. Liu, 2020: Future changes and controlling factors of the eight regional monsoons projected by cmip6 models. J. Climate, 33, 9307-9326, https://doi.org/10.1175/jcli-d-20-0236.1.

Khan, M.A., Spicer, R.A., Bera, S., Ghosh, R., Yang, J., Spicer, T.E.V., Guo, S., Su, T., Jacques, F., Grote, P.J., 2014. Miocene to Pleistocene floras and climate of the Eastern Himalayan Siwaliks, and new palaeoelevation estimates for the Namling–Oiyug Basin, Tibet. Global and Planetary Change 113, 1–10. https://doi.org/10.1016/j.gloplacha.2013.12.003

Kitoh, A., 2002. Effects of Large-Scale Mountains on Surface Climate. A Coupled Ocean-Atmosphere General Circulation Model Study. Journal of the Meteorological Society of Japan 80, 1165–1181. https://doi.org/10.2151/jmsj.80.1165

Kong, Y., Y. Wu, X. Hu, Y. Li, and S. Yang, 2022: Uncertainty in projections of the south Asian summer monsoon under global warming by cmip6 models: Role of tropospheric meridional thermal contrast. Atmospheric and Oceanic Science Letters, 15, 100145, https://doi.org/https://doi.org/10.1016/j.aosl.2021.100145.

Krapp, M., and J. H. Jungclaus, 2011: The middle miocene climate as modelled in an atmosphere-ocean-biosphere model. Climate Past, 7, 1169-1188, https://doi.org/10.5194/cp-7-1169-2011.

Kutzbach, J.E., Guetter, P.J., Ruddiman, W.F., Prell, W.L., 1989. Sensitivity of climate to late Cenozoic uplift in southern Asia and the American west: Numerical experiments. Journal of Geophysical Research: Atmospheres 94, 18393–18407. https://doi.org/10.1029/JD094iD15p18393

Lawrence, D.M., Oleson, K.W., Flanner, M.G., Thornton, P.E., Swenson, S.C., Lawrence, P.J., Zeng, X., Yang, Z.-L., Levis, S., Sakaguchi, K., Bonan, G.B., Slater, A.G., 2011. Parameterization improvements and functional and structural advances in Version 4 of the Community Land Model. Journal of Advances in Modeling Earth Systems 3, M03001. https://doi.org/10.1029/2011MS00045

Licht, A., and Coauthors, 2014: Asian monsoons in a late eocene greenhouse world. Nature, 513, 501-506, https://doi.org/10.1038/nature13704.

Liu, X., and B. Dong, 2013: Influence of the tibetan plateau uplift on the asian monsoon-arid environment evolution. Chinese Science Bulletin, 58, 4277-4291, https://doi.org/10.1007/s11434-013-5987-8.

Liu, X., Xu, Q., Ding, L., 2016. Differential surface uplift: Cenozoic paleoelevation history of the Tibetan Plateau. Sci. China Earth Sci. 59, 2105–2120. https://doi.org/10.1007/s11430-015-5486-y

Liu, Y., Wang, Z., Zhuo, H., Wu, G., 2017. Two types of summertime heating over Asian large-scale orography and excitation of potential-vorticity forcing II. Sensible heating over Tibetan-Iranian Plateau. Sci. China Earth Sci. 60, 733–744. https://doi.org/10.1007/s11430-016-9016-3

Manabe, S., Terpstra, T.B., 1974. The Effects of Mountains on the General Circulation of the Atmosphere as Identified by Numerical Experiments. Journal of the Atmospheric Sciences 31, 3–42. https://doi.org/10.1175/1520-0469(1974)031<0003:TEOMOT>2.0.CO;2

Macgregor, D., 2015: History of the development of the east african rift system: A series of interpreted maps through time. Journal of African Earth Sciences, 101, 232-252, https://doi.org/10.1016/j.jafrearsci.2014.09.016.

McQuarrie, N., Stock, J.M., Verdel, C., Wernicke, B.P., 2003. Cenozoic evolution of Neotethys and implications for the causes of plate motions. Geophysical Research Letters 30. https://doi.org/10.1029/2003GL017992

Medina, S., Houze Jr., R.A., Kumar, A., Niyogi, D., 2010. Summer monsoon convection in the Himalayan region: terrain and land cover effects. Quarterly Journal of the Royal Meteorological Society 136, 593–616. https://doi.org/10.1002/qj.601

Miao, Y., Fang, X., Sun, J., Xiao, W., Yang, Y., Wang, X., Farnsworth, A., Huang, K., Ren, Y., Wu, F., Qiao, Q., Zhang, W., Meng, Q., Yan, X., Zheng, Z., Song, C., Utescher, T., 2022. A new biologic paleoaltimetry indicating Late Miocene rapid uplift of northern Tibet Plateau. Science 378, 1074–1079. https://doi.org/10.1126/science.abo2475

Mouthereau, F., 2011. Timing of uplift in the Zagros belt/Iranian plateau and accommodation of late Cenozoic Arabia–Eurasia convergence. Geological Magazine 148, 726–738. https://doi.org/10.1017/S0016756811000306

Neale, R.B., Richter, J., Park, S., Lauritzen, P.H., Vavrus, S.J., Rasch, P.J., Zhang, M., 2013. The Mean Climate of the Community Atmosphere Model (CAM4) in Forced SST and Fully Coupled Experiments. Journal of Climate 26, 5150–5168. https://doi.org/10.1175/JCLI-D-12-00236.1

Prell, W. L., and J. E. Kutzbach, 1992: Sensitivity of the indian monsoon to forcing parameters and implications for its evolution. Nature, 360, 647-652, https://doi.org/10.1038/360647a0.

Ramstein, G., Fluteau, F., Besse, J., Joussaume, S., 1997. Effect of orogeny, plate motion and land-sea distribution on Eurasian climate change over the past 30 million years. Effect of orogeny, plate motion and land-sea distribution on Eurasian climate change over the past 30 million years 386, 788–795.

Reuter, M., W. E. Piller, M. Harzhauser, and A. Kroh, 2013: Cyclone trends constrain monsoon variability during late oligocene sea level highstands (kachchh basin, nw india). Climate

Past, 9, 2101-2115, https://doi.org/10.5194/cp-9-2101-2013.

Rögl, F., 1997. Palaeogeographic Considerations for Mediterranean and Paratethys Seaways (Oligocene to Miocene). Annalen des Naturhistorischen Museums in Wien. Serie A für Mineralogie und Petrographie, Geologie und Paläontologie, Anthropologie und Prähistorie 99, 279–310.

Sarr, A.-C., and Coauthors, 2022: Neogene south asian monsoon rainfall and wind histories diverged due to topographic effects. Nat Geosci, 15, 314-+, https://doi.org/10.1038/s41561-022-00919-0.

Smith, R., P. Jones, B. Briegleb, F. Bryan, and S. Yeager, 2010: The parallel ocean program (pop) reference manual: Ocean component of the community climate system model (ccsm).

Steinthorsdottir, M., Coxall, H., De Boer, A., Huber, M., Barbolini, N., Bradshaw, C., Burls, N., Feakins, S., Gasson, E., Henderiks, J., Holbourn, A.E., Kiel, S., Kohn, M., Knorr, G., Kürschner, W.M., Lear, C.H., Liebrand, D., Lunt, D.J., Mörs, T., Pearson, P., Pound, M.J., Stoll, H., Stromberg, C., 2021. The Miocene: The Future of the Past. Paleoceanography and Paleoclimatology 36. https://doi.org/10.1029/2020PA004037

Stoker, M.S., Praeg, D., Hjelstuen, B.O., Laberg, J.S., Nielsen, T., Shannon, P.M., 2005. Neogene stratigraphy and the sedimentary and oceanographic development of the NW European Atlantic margin. Marine and Petroleum Geology, The STRATAGEM Project 22, 977–1005. https://doi.org/10.1016/j.marpetgeo.2004.11.007

Su, B., Jiang, D., Zhang, R., Sepulchre, P., Ramstein, G., 2018. Difference between the North Atlantic and Pacific meridional overturning circulation in response to the uplift of the Tibetan Plateau. Climate of the Past 14, 751–762. https://doi.org/10.5194/cp-14-751-2018

Sun, J., Sheykh, M., Ahmadi, N., Cao, M., Zhang, Z., Tian, S., Sha, J., Jian, Z., Windley, B.F., Talebian, M., 2021. Permanent closure of the Tethyan Seaway in the northwestern Iranian Plateau driven by cyclic sea-level fluctuations in the late Middle Miocene. Palaeogeography, Palaeoclimatology, Palaeoecology 564, 110172. https://doi.org/10.1016/j.palaeo.2020.110172

Sun, Y., and Coauthors, 2023: Revisiting the physical mechanisms of east Asian summer monsoon precipitation changes during the mid-Holocene: A data–model comparison. Climate Dynamics, 60, 1009-1022, https://doi.org/10.1007/s00382-022-06359-1.

Tada, R., H. Zheng, and P. D. Clift, 2016: Evolution and variability of the asian monsoon and its potential linkage with uplift of the himalaya and tibetan plateau. Progress in Earth and Planetary Science, 3, https://doi.org/10.1186/s40645-016-0080-y.

Tan, M., Zhu, X., Liu, Q., Zhang, Z., Liu, W., 2020. Multiple fluvial styles in Late Miocene post-rift successions of the offshore Bohai Bay Basin (China): Evidence from a seismic geomorphological study. Marine and Petroleum Geology 113, 104173. https://doi.org/10.1016/j.marpetgeo.2019.104173

Tang, H., Micheels, A., Eronen, J.T., Ahrens, B., Fortelius, M., 2013. Asynchronous responses of East Asian and Indian summer monsoons to mountain uplift shown by regional climate modelling experiments. Clim Dyn 40, 1531–1549. https://doi.org/10.1007/s00382-012-1603-x

Tardif, D., Fluteau, F., Donnadieu, Y., Le Hir, G., Ladant, J.-B., Sepulchre, P., Licht, A., Poblete, F., Dupont-Nivet, G., 2020. The origin of Asian monsoons: a modelling perspective. Climate of the Past 16, 847–865. https://doi.org/10.5194/cp-16-847-2020

Tardif, D., and Coauthors, 2023: The role of paleogeography in Asian monsoon evolution: A review and new insights from climate modelling. Earth-Science Reviews, 243, 104464, https://doi.org/https://doi.org/10.1016/j.earscirev.2023.104464.

The Cenozoic, C. O. P. I. P. C., and Coauthors: Toward a Cenozoic history of atmospheric co2. Science, 382, eadi5177, https://doi.org/10.1126/science.adi5177.

Thomson, J. R., P. B. Holden, P. Anand, N. R. Edwards, C. A. Porchier, and N. B. W. Harris,

2021: Tectonic and climatic drivers of asian monsoon evolution. Nat. Commun., 12, 4022, https://doi.org/10.1038/s41467-021-24244-z.
Vogeli, N., P. Huyghe, P. van der Beek, Y. Najman, E. Garzanti, and C. Chauvel, 2017: Weathering regimein the eastern himalaya since the mid-miocene: Indications fromdetrital geochemistry and claymineralogy of the kameng river section, arunachal pradesh, india. Basin Research, 30, 59-74, https://doi.org/10.1111/bre.12242.
Wang, C., Dai, J., Zhao, X., Li, Y., Graham, S.A., He, D., Ran, B., Meng, J., 2014. Outward-growth of the Tibetan Plateau during the Cenozoic: A review. Tectonophysics 621, 1–43. https://doi.org/10.1016/j.tecto.2014.01.036
Wang, Z., Duan, A., Yang, S., 2019. Potential regulation on the climatic effect of Tibetan Plateau heating by tropical air–sea coupling in regional models. Clim Dyn 52, 1685–1694. https://doi.org/10.1007/s00382-018-4218-z
Wu, G., Liu, Y., He, B., Bao, Q., Duan, A., Jin, F.-F., 2012. Thermal Controls on the Asian Summer Monsoon. Scientific Reports 2, 404. https://doi.org/10.1038/srep00404
Wu, G., Liu, Y., Zhang, Q., Duan, A., Wang, T., Wan, R., Liu, X., Li, W., Wang, Z., Liang, X., 2007. The Influence of Mechanical and Thermal Forcing by the Tibetan Plateau on Asian Climate. Journal of Hydrometeorology 8, 770–789. https://doi.org/10.1175/JHM609.1
Yang, X., Groeneveld, J., Jian, Z., Steinke, S., Giosan, L., 2020. Middle Miocene Intensification of South Asian Monsoonal Rainfall. Paleoceanography and Paleoclimatology 35, e2020PA003853. https://doi.org/10.1029/2020PA003853
Zhang, R., Jiang, D., Liu, X., Tian, Z., 2012. Modeling the climate effects of different subregional uplifts within the Himalaya-Tibetan Plateau on Asian summer monsoon evolution. Chin. Sci. Bull. 57, 4617–4626. https://doi.org/10.1007/s11434-012-5284-y
Zhang, R., Jiang, D., Zhang, Z., 2019. Vegetation and Ocean Feedbacks on the Asian Climate Response to the Uplift of the Tibetan Plateau. Journal of Geophysical Research: Atmospheres 124, 6327–6341. https://doi.org/10.1029/2019JD030503
Zhang, R., Jiang, D., Zhang, Z., Yu, E., 2015. The impact of regional uplift of the Tibetan Plateau on the Asian monsoon climate. Palaeogeography, Palaeoclimatology, Palaeoecology 417, 137–150. https://doi.org/10.1016/j.palaeo.2014.10.030

Table 1. Simulations performed with CESM1.2 in this study. See Fig.2 for modern and paleogeography maps.

experiment	Geolography	vegetation	CO2 (ppm)	IP	HM
piControl	Modern	Modern	280	Modern	Modern
MMIO (IP100HM80)	M.Miocene*	M.Miocene	400	M.Miocene	M.Miocene
IP0HM0	M.Miocene	M.Miocene	400	0	0
IP50HM0	M.Miocene	M.Miocene	400	50%	0
IP100HM0	M.Miocene	M. Miocene	400	100%	0
IP0HM100	M.Miocene	M.Miocene	400	0	100%**
IP50HM100	M.Miocene	M.Miocene	400	50%	100%
IP100HM100	M. Miocene	M. Miocene	400	100%	100%
MMIO280	M. Miocene	M.Miocene	280	M. Miocene	M.Miocene
MMIO560	M. Miocene	M.Miocene	560	M. Miocene	M.Miocene
MMIO800	M. Miocene	M.Miocene	800	M. Miocene	M.Miocene
MMIO1000	M.Miocene	M.Miocene	1000	M. Miocene	M.Miocene

*M.Miocene: Middle Miocene

** 100% of the height of modern HM.

Table 2. Evidence of modern SAM in middle Miocene from recently published studies.

No	station	Location (lat/lon)	Proxies	Intensification age (Ma)	Trend*	variable	references
1	Well Indus Marine A-1	24/66	weathering	15~12	decreasing	Precip	Clift et al., 2008
2	ODP 359	5/73	Sedimentary& geochemical record	12.9	increasing	wind	Betzler et al., 2016
3	ODP 722B	16.6/59.8	Bio-marker	12.9	increasing	wind	Gupta et al., 2015
	ODP 722B	16.6/59.8	Bio-marker	14	increasing	wind	Bialik et al., 2020
4	NGHP-01-01A	15/71	Bio-marker	14	increasing	Precip	Yang et al., 2020
5	Varkala	8.7/76.7	Pollen fossil	17-15	No change	Precip.	Reuter et al., 2013
6	ODP 758	5.4/90.4	weathering	13.9	increasing	wind	Ali et al., 2021
7	Surai Khola	27.8/83	Leaf Fossil	13	increasing	Precip.	Srivastava et al., 2018 Bhatia et al., 2021
8	Darjeeling	27/88.5	Leaf Fossil	13	increasing	Precip.	Khan et al., 2014
9	Arunachal Pradesh	27/93.5	Leaf Fossil	13	No change	Precip.	Khan et al., 2014
	Arunachal Pradesh	26/93.5	weathering	13	No change	Precip.	Vogeli et al., 2017

* Trend of monsoon index change from middle to late Miocene.